Environmental Pollution 292 (2022) 118412

Contents lists available at ScienceDirect

Environmental Pollution

journal homepage: www.elsevier.com/locate/envpol

Enhanced removal of ammonium from water using sulfonated reed waste biochar-A lab-scale investigation☆

Ming Zhang [a], Ruyi Sun [a], Ge Song [a], Lijun Wu [b], Hui Ye [c], Liheng Xu [a], Sanjai J. Parikh [d], Tuan Nguyen [e], Eakalak Khan [f], Meththika Vithanage [g], Yong Sik Ok [h,*]

[a] Department of Environmental Engineering, China Jiliang University, Hangzhou, 310018, Zhejiang, China
[b] China Huadong Engineering Corporation Limited, Hangzhou, Zhejiang, 311122, China
[c] Hangzhou Environmental Monitoring Central Station, Hangzhou, 310007, Zhejiang, China
[d] Department of Land, Air and Water Resources, University of California –Davis, Davis, CA, 95618, USA
[e] Centre for Mined Land Rehabilitation, Sustainable Minerals Institute, The University of Queensland, Brisbane, QLD, 4072, Australia
[f] Civil and Environmental Engineering and Construction Department, University of Nevada, Las Vegas, NV, 89154-4015, USA
[g] Ecosphere Resilience Research Center, Faculty of Applied Sciences, University of Sri Jayewardenepura, Nugegoda, 10250, Sri Lanka
[h] Korea Biochar Research Center, APRU Sustainable Waste Management Program & Division of Environmental Science and Ecological Engineering, Korea University, Seoul, Republic of Korea

ARTICLE INFO

Keywords:
Biochar
Ammonium
Adsorption
Sulfonation
Engineered biochar
Water treatment

ABSTRACT

The removal of excessive ammonium from water is vital for preventing eutrophication of surface water and ensuring drinking water safety. Several studies have explored the use of biochar for removing ammonium from water. However, the efficacy of pristine biochar is generally weak, and various biochar modification approaches have been proposed to enhance adsorption capacity. In this study, biochar obtained from giant reed stalks (300, 500, 700 °C) was modified by sulfonation, and the ammonium adsorption capabilities of both giant reed biochars (RBCs) and sulfonated reed biochars (SRBCs) were assessed. The ammonium adsorption rates of SRBCs were much faster than RBCs, with equilibrium times of ~2 h and ~8 h for SRBCs and RBCs, respectively. The Langmuir maximum adsorption capacities of SRBCs were 4.20–5.19 mg N/g for SRBCs, significantly greater than RBCs (1.09–1.92 mg N/g). Physical-chemical characterization methods confirmed the increased levels of carboxylic and sulfonic groups on sulfonated biochar. The reaction of ammonium with these O-containing functional groups was the primary mechanism for the enhancement of ammonium adsorption by SRBCs. To conclude, sulfonation significantly improved the adsorption performance of biochar, suggesting its potential application for ammonium mitigation in water.

1. Introduction

Owing to rapid worldwide industrial development and agricultural expansion, excessive anthropogenic ammonium inputs from industrial effluents, domestic discharge, and agricultural runoff into aquatic systems have elevated the risk of eutrophication in water bodies, including rivers, lakes, estuaries, reservoirs, and oceans (Conley et al., 2009; Woodward et al., 2012; Xia et al., 2020). Therefore, ammonium removal from water and wastewater is vital. Biological processes are the most widely adopted techniques that convert ammonium into nitrite and nitrate under aerobic conditions and subsequent reduction to N_2 under anaerobic conditions (Maranon et al., 2006). Physicochemical methods (i.e., air stripping or magnesium ammonium phosphate precipitation) have also been adopted to treat wastewater with high ammonium concentrations (Zhang et al., 2011).

In the past decades, researchers have focused on the application of adsorbents, such as clay minerals (Alshameri et al., 2018), volcanic tuff (Maranon et al., 2006), zeolites (Niu et al., 2012), polymeric exchangers (Jorgensen and Weatherley, 2003), and biochars (Gai et al., 2014; Hale et al., 2013; Zeng et al., 2013), to remove ammonium from wastewater. Biochar, a C-rich solid residue produced by the thermal pyrolysis of biomass waste (Ahmad et al., 2014), has gained much attention as a low-cost adsorbent. Biochar has high cation exchange capacity (CEC) and significant O-containing functional groups (OFG), which are

☆ This paper has been recommended for acceptance by SU SHIUNG LAM.
* Corresponding author.
E-mail address: yongsikok@korea.ac.kr (Y.S. Ok).

https://doi.org/10.1016/j.envpol.2021.118412
Received 3 August 2021; Received in revised form 24 October 2021; Accepted 26 October 2021
Available online 28 October 2021

considered to promote ammonium adsorption (Yang et al., 2017; Seredych and Bandosz, 2007). Former studies have shown that biochar ammonium adsorption capacities vary significantly based on the feedstock type and the pyrolysis conditions (Fan et al., 2019; Kizito et al., 2015; Hou et al., 2016), some of which yielded biochars that interacted only weakly with ammonium (Hou et al., 2016).

To further enhance biochar's capability for ammonium adsorption, various biochar modifications have been attempted based on two primary strategies. Increasing the CEC of biochar can provide more exchangeable cations for ammonium (Chen et al., 2017; Ismadji et al., 2015; Gong et al., 2017). For instance, Gong et al. found that Mg-modified biochar offered significantly higher NH_4^+ adsorption, associated with the exchange of Mg^{2+} (Gong et al., 2017). Moreover, introducing OFG on the biochar surface may promote more chemical bonding or electrostatic interactions with ammonium because biochar with a higher O/C mole ratio has demonstrated higher ammonium adsorption capacities (Yang et al., 2017). Zhang et al. reviewed the reported performance of biochars on the removal of ammonium from water and found that the modified biochars had a much higher adsorption capacity (22.78 mg N/g average) compared to the unmodified ones (11.19 mg N/g) (Zhang et al., 2020). Besides, biochar sulfonation has also been reported for incorporating $–SO_3H$ on biochar surface, which has been used as a catalyst in recent studies (Cao et al., 2018; Hidayat et al., 2015; Xiong et al., 2018).

Giant reeds (*Arundo donax* L.) were selected as the biochar feedstock. This plant is geographically widespread in China and is frequently used in constructed wetlands for water and wastewater treatment because of its rapid growth, resistance to drought and flooding, and high yields (Hou et al., 2016; Zheng et al., 2013). Further, the proper disposal of giant reed waste after harvest from constructed wetlands in autumn/-winter is urgent. We hypothesized that introducing O-containing functional groups to biochar surfaces, such as $–SO_3H$ via sulfonation, can enhance the adsorption of ammonium. Therefore, this study aimed to: (1) compare the ammonium adsorption capacities of biochar produced at 300, 500, and 700 °C from giant reed stalks (RBC) and its counterpart after sulfonation (SRBC); (2) characterize the surface properties, particularly the surface functional groups of the RBC and SRBC; and (3) investigate the mechanisms of the ammonium adsorption enhancement. Results are expected to elucidate the possible fundamental mechanisms of ammonium adsorption by biochar and highlight the potential application of modified biochar for water-quality control.

2. Materials and methods

2.1. Preparation of pristine and sulfonated biochar

The giant reed stalks were harvested from a wetland in Zhejiang Province, China. It was washed with tap water to remove impurities and then dried at 60 °C for 24 h. The dried reed stalks were crushed using a tissue masher and sieved for fine powder (<100 mesh), which was then pyrolyzed in a customized quartz container using a muffle furnace (Nabertherm B180) at peak temperatures of 300, 500, and 700 °C with the heating rate of 5 °C/min under continuous gentle N_2 purging (100 mg/min) (Fig. S1). Before pyrolysis, N_2 was purged in advance (100 mL/min) for about 30 min to ensure a near-oxygen-free environment. Samples were kept at peak temperature for 1 h, then cooling down to room temperature for further use. During the whole pyrolysis process, including cooling down, the chamber was purged by gentle N_2 continuously with the same flow rate of 100 mL/min. The reed biochars (RBCs) pyrolyzed at these three temperatures are denoted as RBC300, RBC500, and RBC700.

RBC sulfonation was performed via a thermal reaction with concentrated sulfuric acid. In detail, RBCs were individually mixed with 98% H_2SO_4 at a solid-to-liquid ratio of 1:15 (g:mL) at 150 °C in a glass reactor, and the mixtures were magnetically stirred for 12 h. The solid residue was washed in hot water repeatedly until the washing effluent reached a neutral pH. The solid residues were then dried at 60 °C for 48 h, and the final sulfonated reed biochars (SRBCs) derived from RBC300, RBC500, and RBC700 were denoted as SRBC300, SRBC500, and SRBC700, respectively.

2.2. Adsorption experiments

Ammonium chloride (NH_4Cl, Sinopharm Chemical Reagent Co.) was used to prepare the ammonium solution for adsorption experiments. 100 mg N/L NH_4Cl was prepared with distilled water as the stock solution, and the other concentrations of ammonium used in the adsorption experiments were diluted from the stock solution. Solution chemistry was not adjusted further. The final concentrations of ammonium in all samples, including controls, were determined using a national standard method of China: salicylic acid spectrophotometry with a detection limit of 0.01 mg/L and a sensitivity of 0.04 mg/L to 1.00 mg/L (10 mm cell). The ammonia and ammonium ions in the water can react with the salicylate and hypochlorite ions in the presence of sodium nitroprusside under alkaline condition (pH = 11.7). A blue compound was generated and was determined by a spectrophotometer at a wavelength of 697 nm. (Ministry of Environmental Protection, 2009). All the ammonium concentrations above 1.0 mg/L were diluted into this concentration range for the best accuracy.

2.2.1. Adsorption kinetics

The adsorption kinetics were carried out using batch experiments. Each sample contained 20 mL ammonium solution (5 mg N/L) along with 0.05 g RBC or 0.02 g SRBC and was sealed in a 22 mL glass tube with a Teflon-sealed cap. Duplicate samples along with duplicate control samples without RBC or SRBC were prepared for each time interval (0, 0.25, 0.5, 0.75, 1.0, 2.0, 4.0, 6.0, 8.0, 12.0, 16.0, and 24.0 h). Samples were shaken at 25 ± 0.5 °C at 150 rpm, collected at each time interval, and filtered by a 13 mm*0.22 μm hydrophilic polyethersulfone (PES) syringe filter before NH_4^+ analysis. The amount of NH_4^+ adsorbed by the biochars at each time interval was calculated based on the following equation:

$$Q_t = \frac{(C_0 - C_t)V}{m} \quad \text{(Eq. 1)}$$

where Q_t is the adsorbed amount of NH_4^+ (mg N/g) at time t, and C_0 and C_t are the initial and equilibrium NH_4^+ concentrations (mg N/L) at time t, respectively. V and m are the solution volume (L) and mass (g) of biochar in each sample, respectively.

The pseudo-first-order (PFO) kinetic model (Eq. (2)) was first suggested by Lagergren (1898) to describe the liquid-to-solid adsorption rate, and the pseudo-second-order (PSO) kinetic model (Eq. (3)) was suggested by Ho (Ho, 1995; Ho and McKay, 1999) when chemisorption occurred. Both are often applied as potential prediction models to fit adsorption kinetics data, and they were both used to fit the determined kinetics data.

$$Q_t = Q_{e1}(1 - e^{-k_1 t}) \quad \text{(Eq. 2)}$$

$$Q_t = \frac{k_2 Q_{e2}^2 t}{1 + k_2 Q_{e2} t} \quad \text{(Eq. 3)}$$

where k_1 and k_2 are the rate constants for first-order and second-order, respectively, and Q_{e1} and Q_{e2} are the maximum adsorption amounts estimated by the PFO and PSO kinetic models, respectively.

2.2.2. Adsorption isotherms

Adsorption isotherms were studied via batch adsorption experiments. Biochar (0.1 g for RBCs and 0.02 g for SRBCs) was mixed with 20.0 mL ammonium solutions with varying N concentrations (1–15 mg N/L) at 25 ± 0.5 °C in 22 mL glass tubes with Teflon-sealed caps. After shaking for 24 h at 150 rpm, samples were filtered using 0.22 μm

hydrophilic syringe filters before ammonium analysis. All samples were conducted in duplicate, and the control samples without biochar were also prepared. The classic Langmuir adsorption model (Eq. (4)), which describes monolayer adsorption behavior and an adsorption maximum, was employed to fit the non-linear adsorption isotherms.

$$Q_e = \frac{Q_m K_L C_e}{1 + K_L C_e} \quad \text{(Eq. 4)}$$

where Q_e is the adsorbed amount of ammonium (mg N/g) by biochars at equilibrium concentration C_e (mg N/L), K_L is the Langmuir adsorption constant, and Q_m (mg N/g) is the estimated adsorption capacity of the biochar.

2.3. Characterization of RBCs and SRBCs

The morphology of RBCs and SRBCs was observed by applying field-emission scanning electron microscopy (FE-SEM, Hitachi SU-8010) with Pt-coated to samples, and all FE-SEM images were recorded at 10.0 kV.

The surface areas of the biochars were analyzed using the N_2 adsorption-desorption method with a surface area analyzer (Micromeritics Gemini VII, USA). All samples were degassed at 90 °C and 200 °C before measurement. The surface areas were determined via multipoint analysis of the N_2 adsorption and desorption, and the Brunauer–Emmett–Teller (BET) surface areas were recorded. Standard samples with known surface areas were analyzed for quality control and the RBC and SRBC samples. The biochars' elemental compositions (C, S, O, H, N) were determined using an elemental analyzer (Vario EL Cube, UK).

Fourier-transform infrared spectroscopy (FTIR) data was collected over a wavenumber range of 4000–400 cm^{-1} using a Thermo Fisher Nicolet iS 5 spectrometer and deuterated-triglycine sulfate detector with a 4 cm^{-1} resolution. The samples (about 2 mg) were mixed in KBr (about 200 mg) powder and then grounded fully and pressed to a transparent pellet before analysis. Transmission analysis was conducted on KBr pellets to characterize biochar's the functional groups. X-ray

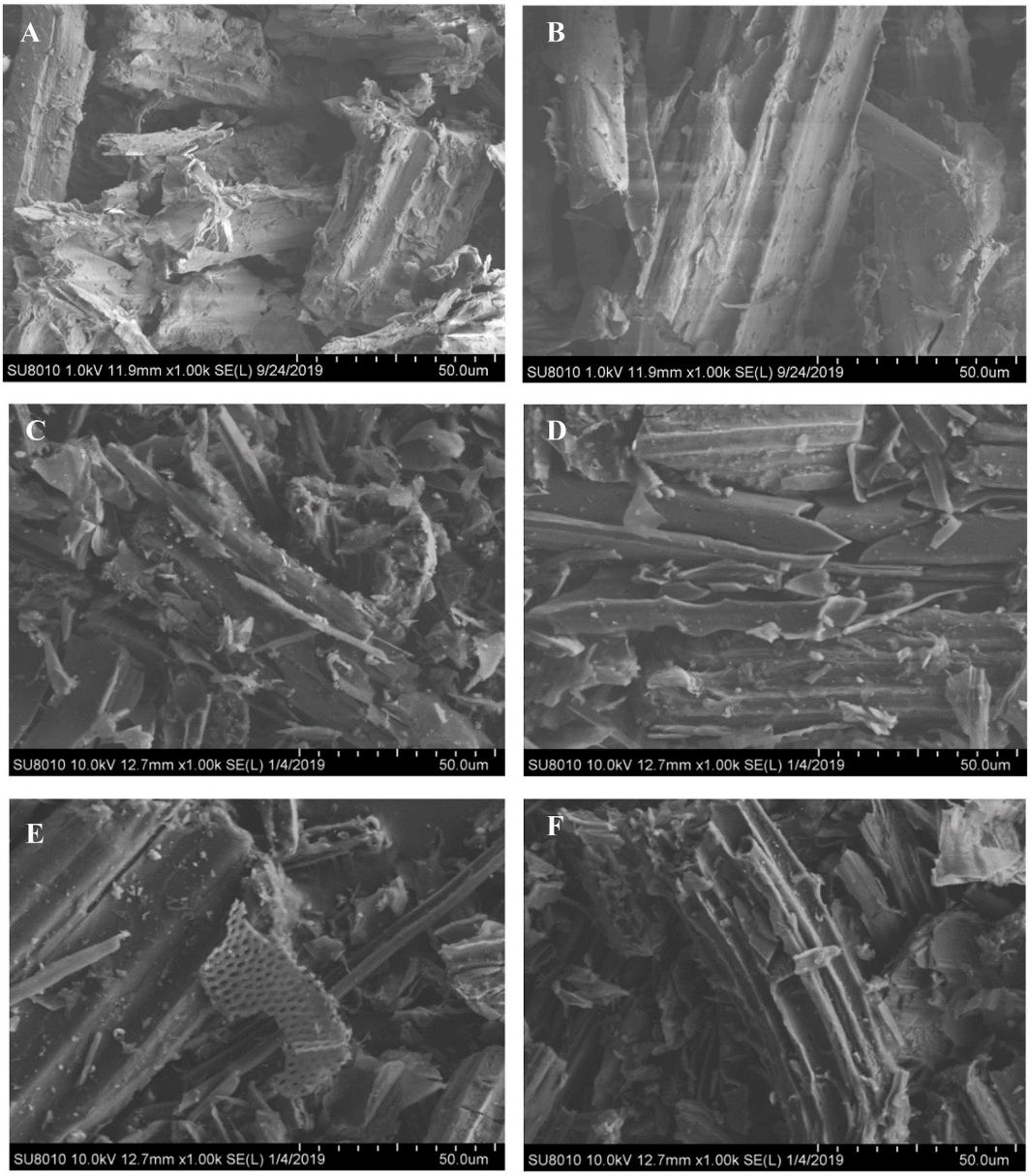

Fig. 1. The Scanning electron microscopy images of giant reed biochars (RBCs) and sulfonated RBCs (SRBCs). A) RBC300; B) SRBC300; C) RBC500; D) SRBC500; E) RBC700; F) SRBC700.

photoelectron spectroscopy (XPS) was tested using a Thermo Scientific K-alpha + spectrometer to analyze the chemical states of the selected elemental compositions.

3. Results and discussion

3.1. Morphology of RBCs and SRBCs

The morphologies of RBCs and SRBCs were observed via scanning electron microscopy (SEM, Fig. 1). There were no apparent differences among RBCs pyrolyzed at different temperatures and all RBCs (Fig. 1). Within the pyrolysis temperature range (from 300 to 700 °C), no visible pore structures formed on the biochar surface. Although studies reported that biochars' surface area (SA) generally increases with an increase in pyrolysis temperature due to the decomposition of organic components in the biomass (Ahmad et al., 2014), the SAs of RBCs were not found to correlate with the pyrolysis temperature. RBCs pyrolyzed at 300–700 °C in this study had very low SAs, ranging from 2.63 to 39.51 m^2/g with pore volumes of 0.005–0.016 cm^3/g (Table S1). This result is consistent with the observation reported by Zheng et al. (2013), who found that the SAs of biochars derived from giant reeds (a species similar to those considered in this study) at 300–600 °C ranged from 2.16 to 50 m^2/g. The similarity of these results might reflect the properties and characteristics of the feedstock reeds.

As noted, the surface morphology of the SRBCs (Fig. 1B, D, F) also showed no significant differences with their RBC counterparts at the same pyrolysis temperature, indicating that sulfonation with concentrated sulfuric acid did not alter the physical morphology of biochar. Meanwhile, the sulfonation process did not etch the biochar surface or create new pore structures, as indicated by the similarly low surface areas (4.17–13.31 m^2/g) and low pore volumes (0.010–0.022 cm^3/g) of SRBCs and RBCs. These results imply that differences in ammonium adsorption between RBCs and SRBCs could not be attributed to differences in their surface areas.

3.2. Adsorption kinetics

The kinetics of ammonium adsorption by RBCs and SRBCs were examined at ammonium concentrations of 5 mg N/L at different time intervals to investigate the adsorption rate and equilibrium time (Fig. 2). For all RBCs and SRBCs, a sharp Q_t increase was observed at the beginning of adsorption, especially in the first 2 h, indicating higher initial adsorption potentials due to the maximal concentration differences between the adsorbent and solution. After that, the curves gradually reached a plateau, showing that the adsorption approached equilibrium. Although both PFO and PSO kinetic models fit the determination data well, and the PSO kinetic model performed much better with R^2 values higher than 0.94 (Table 1). This indicates that the adsorption of ammonium by RBCs and SRBCs may be via chemisorption. Notably, SRBCs reached equilibrium more quickly than RBCs. Fig. 2 shows that the equilibrium time for RBCs was approximately 8 h, while it was only about 2 h for SRBCs. In addition, the much higher k_1 and k_2 values of SRBCs than those of RBCs also indicated faster ammonium adsorption by SRBCs than by RBCs (Table 1). For example, the k_1 values of RBCs were 0.61–0.98 h^{-1}, while they were 2.09–5.34 h^{-1} for SRBCs. The same trend was also applicable for k_2. Gong et al. (2017) reported that the equilibrium time of ammonium adsorption by $MgCl_2$-modified *Phragmites australis* biochar was approximately 10 h, and the kinetic curve fit the PSO model well. Thus, it can be inferred that chemisorption, including reactions with polar functional groups on the biochar surface and cation exchange, is the main mechanism for ammonium adsorption (Gong et al., 2017). Similarly, ammonium adsorption by pine sawdust and wheat straw biochars (300 °C and 500 °C) reached equilibrium in 12 h (Yang et al., 2017). Compared with these results, the SRBCs in this study had a much faster adsorption rate, suggesting that they could be feasibly applied for water or wastewater treatment. Fig. 2 also shows that the equilibrium adsorption amounts of SRBCs were significantly higher than those of RBCs at the same initial ammonium concentration. RBC and SRBC pyrolyzed at 300 °C had higher adsorption capacities for ammonium than those pyrolyzed at 500 °C and 700 °C.

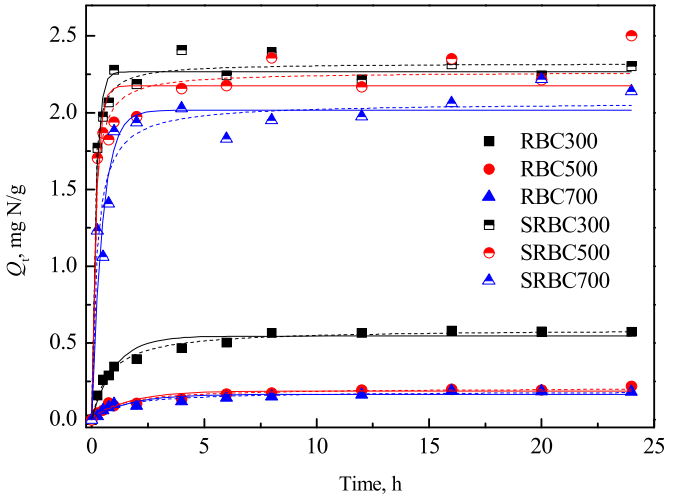

Fig. 2. Adsorption kinetics of ammonium by giant reed biochars (RBCs) and sulfonated RBCs (SRBCs). The solid lines fit the pseudo-first-order kinetic model, and the dashed lines fit the pseudo-second-order kinetic model.

3.3. Adsorption isotherms

The ammonium adsorption isotherm experiments were conducted at initial ammonium concentrations of 0–15 mg N/L for both RBCs and SRBCs, and the results are shown in Fig. 3. Isotherm curves are typically non-linear, indicating surface-based adsorption patterns rather than partitioning into the biochar matrix. At low ammonium concentrations, the adsorption sites on the biochars were abundant, and the amounts of ammonium adsorbed increased sharply. With a further increase in the ammonium concentration in the aqueous phase, fewer adsorption sites became available, and the isotherm curves tended to bend and level off. Subsequently, the adsorption sites on biochar surfaces became saturated, and maximum adsorption was reached. As a result, the Langmuir model, based on monolayer adsorption, was employed to fit the isotherm curves and estimate the maximum adsorption capacities (Q_m) of each biochar. The estimated adsorption parameters obtained from Langmuir fitting are listed in Table 2. The correlation coefficients (R^2) were all above 0.94, indicating that the Langmuir model can effectively fit the adsorption behavior of ammonium on RBCs and SRBCs.

As shown in Fig. 3, for RBCs, the isotherm curve of RBC300 was significantly above those of RBC500 and RBC700, and RBC500 was slightly higher than RBC700 in the tested concentration range. Thus, the apparent adsorption capacity order is RBC300 ≫ RBC500 > RBC700. The Langmuir model estimated Q_m of RBC300 was 1.92 mg N/g, higher

Table 1
Pseudo-first-order and pseudo-second-order kinetic model parameters of ammonium adsorption by biochars.

Biochars	Pseudo-first-order kinetic model			Pseudo-second-order kinetic model		
	k_1, h^{-1}	Q_{e1}, mg N/g	R^2	k_2, g·mg^{-1} h^{-1}	Q_{e2}, mg N/g	R^2
RBC300	0.98	0.54	0.9497	2.22	0.59	0.9884
RBC500	0.61	0.19	0.8869	3.81	0.21	0.9468
RBC700	0.62	0.17	0.8870	4.15	0.19	0.9457
SRBC300	5.34	2.27	0.9763	5.58	2.32	0.9857
SRBC500	4.89	2.18	0.9097	3.91	2.27	0.9589
SRBC700	2.09	2.02	0.9088	2.24	2.07	0.9552

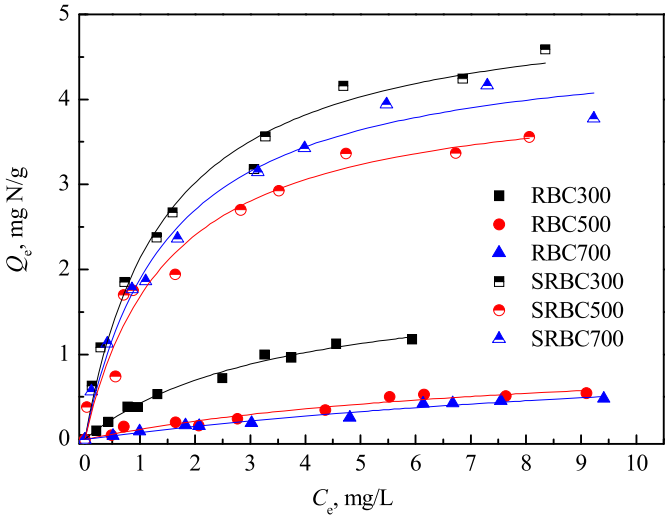

Fig. 3. Adsorption isotherms of ammonium by giant reed biochars (RBCs) and sulfonated RBCs (SRBCs). The solid lines are the Langmuir adsorption model fitted curves.

Table 2
Langmuir isotherm model parameters for the adsorption of ammonium on giant reed biochars (RBCs) and sulfonated RBCs (SRBCs).

Biochars	k_L, L/mg	Q_m, mg/g	R^2
RBC300	0.28	1.92	0.9891
RBC500	0.12	1.09	0.9484
RBC700	0.07	1.30	0.9691
SRBC300	0.69	5.19	0.9858
SRBC500	0.67	4.20	0.9649
SRBC700	0.66	4.74	0.9836

Note: K_L = Langmuir adsorption constant; Q_m = Estimated adsorption capacity of the biochars.

than RBC500 (1.09 mg N/g) and RBC700 (1.30 mg N/g). This trend is consistent with reported results, which indicated that biochar pyrolyzed at lower temperatures has better ammonium adsorption performance. For instance, Gai et al. found a negative correlation between ammonium adsorption and pyrolysis temperature among 12 biochars from three feedstocks at four different pyrolysis temperatures (Gai et al., 2014). It has also been observed that a higher ammonium Q_m for pine sawdust biochar produced at 300 °C than that produced at 550 °C (Yang et al., 2017). The loss of polar functional groups, especially O-containing functional groups such as carboxyls, on the surface of biochar at higher pyrolysis temperatures is believed to be the main reason for the reduced Q_m values (Keiluweit et al., 2010). In addition, Gai et al. (2014) and Yang et al. (2017) have found that the reduced cationic exchange capacity (CEC) at higher pyrolysis temperatures may lead to lower levels of ammonium removal via the reduction of ion exchange.

The Q_m values of SRBCs are much higher than those of RBCs, indicating that biochar sulfonation can significantly enhance the adsorption of ammonium on biochar. For instance, the Q_m of SRBC300 was 5.19 mg N/g, while RBC300 was 1.92 mg N/g (2.7x greater). Similarly, the Q_m values of SRBC500 and SRBC700 3.85 and 3.65 times greater than those of their counterparts RBC500 and RBC700, respectively. After sulfonation, the Q_m differences among SRBCs were not as significant as those among RBCs, indicating that the sulfonation process may be the main contributor to enhance ammonium adsorption capacities of SRBCs.

In our former publication (Zhang et al., 2020), we have summarized the Q_m of biochars for ammonium adsorption in the reported literature and found that the majority of Q_m by unmodified biochars was lower than 5.0 mg N/g, indicating that SRBC had comparable removal capacities with most of the unmodified biochars. However, it is lower than the average Q_m of the modified biochars (22.78 mg N/g average).

3.4. Mechanism of the enhanced adsorption of ammonium by SRBCs

To reveal the enhanced ammonium adsorption mechanisms after sulfonation, detailed comparisons between SRBC300 and its counterpart RBC300 were conducted due to their best performance on ammonium adsorption. We hypothesized that the sulfonation process may have introduced polar functional groups to the biochar surface, leading to stronger interactions and subsequently enhancing the adsorption and removal of ammonium from water. As a result, various approaches were employed to characterize the surface properties of biochar before and after sulfonation, including FTIR, elemental analysis, and XPS.

3.4.1. FTIR

Surface functional groups, especially O-containing functional groups (OFGs), are believed to be predominant in governing the adsorption of ammonium on carbon surfaces. For example, Yang et al. found that low temperature-derived biochar has a higher O/C mole ratio and higher ammonium adsorption capacity than high temperature-derived biochar, and they believed that the chemical interaction or electrostatic attractions between biochar OFGs and NH_4^+ was the main mechanism behind this outcome (Yang et al., 2017). Fig. 4 presents the FTIR spectra of RBC300, SRBC300, and ammonium-bounded SRBC300 from this study. Compared to higher temperatures, biochar produced at 300 °C have more OFGs, and aromatic carbon peaks are less prominent.

The most significant difference between the FTIR spectra of RBC and SRBC is the band at 1174 cm^{-1}. It is reported that the FTIR bands at 1172 and 1031 cm^{-1} of the sulfonated biochar could be ascribed to the

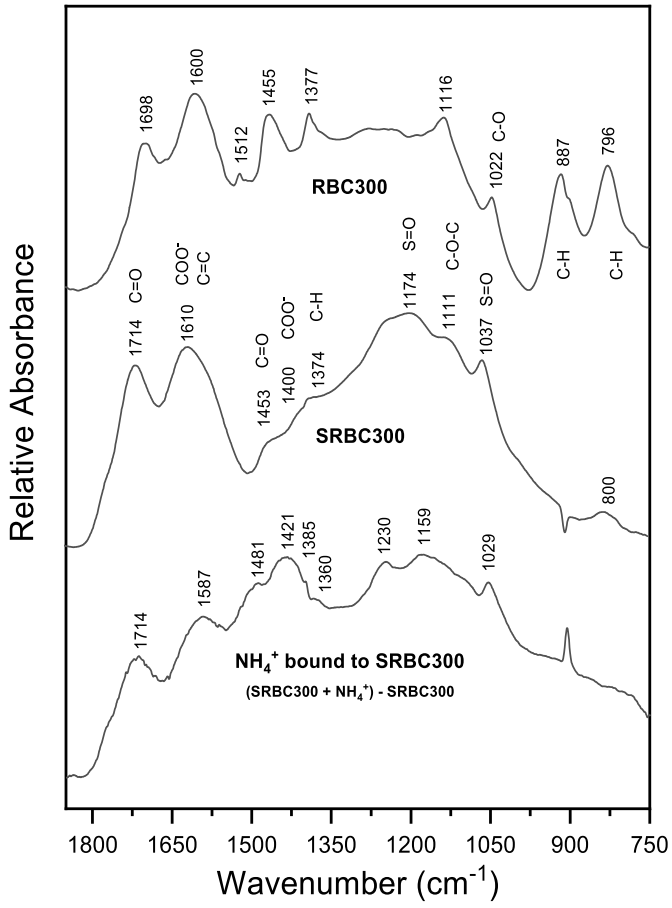

Fig. 4. Fourier-transform infrared absorbance spectra of RBC300, SRBC300, and the difference spectrum of SRBC300 reacted with ammonium and the original SRBC300 spectrum.

S═O stretching modes of –SO_3H (Cao et al., 2018), which corresponds to bands at 1174 and 1037 cm^{-1} for SRBC300 (Fig. 4). These IR bands indicate that –SO_3H was successfully introduced on the SRBC300 surface. Furthermore, the band at 1712 cm^{-1} is attributed to C═O stretching from carboxyls (Hidayat et al., 2015), indicating additional O-containing functional groups (other than –SO_3H) were also introduced on the SRBC300 surface after sulfonation. Both RBC300 and SRBC300 spectra are bands around 1600 and 1400 corresponding to the asymmetric (ν_{as}) and symmetric (ν_{as}) stretching vibrations of carboxyl groups. Additionally, the band at 2924 cm^{-1} of SRBC decreased considerably (see Supporting Information, Fig. S2). This band is part of a quartet of peaks attributed to the symmetric and asymmetric vibrations of –CH_2– and CH_3 in aliphatic chains (Brancaleon et al., 2001; Parikh et al., 2014). Other indications of reduced aliphatic groups are seen with the decreases at 1455, 887, and 796 cm^{-1} (Keiluweit et al., 2010; Hsu and Lo, 1999; Sharma et al., 2004; Ozcimen and Ersoy-Mericboyu, 2010). Since the pyrolysis temperature of RBC300 was 300 °C, a considerable portion of un-carbonized biomass residue containing aliphatic chains remained. After sulfonation, the intensity of bands corresponding to aliphatic groups was significantly decreased due to the dehydration and carbonization effects of the concentrated sulfuric acid, which reduced the presence of C–H bonds of aliphatic chains.

With the increased abundance of OFGs by sulfonation, a higher ammonium adsorption capacity was expected for SRBC300 than RBC300. Examination of the difference spectrum of the sulfonated biochar following reaction with ammonium reveals notable differences are apparent, suggesting inner-sphere complexation. Specifically, a downshift for bands corresponding to –SO_3H, from 1174 to 1157 cm^{-1} and 1037 to 1029 cm^{-1}, and for COO^-, 1610 to 1587 cm^{-1} and 1400 to 1385 cm^{-1}, is observed (Fig. 4). Downward shifts in FTIR band locations, including COO^- and –SO_3H, upon adsorption, is commonly interpreted as evidence for chemical bonds (Hafner and Parikh, 2020; Kang and Xing, 2007; Peak, Ford, and Sparks, 1999; Yang et al., 2007).

3.4.2. Elemental analysis

The introduction of OFGs, such as –SO_3H, –OH, and –COOH, was also reflected in the elemental compositions of RBC300 and SRBC300 (Table 3). The weight fraction of O increased from 18.35% for RBC300 to 33.44% for SRBC300, and that of S rose from 0.35% for RBC300 to 2.73% for SRBC300. The O/C mole ratio was 0.21 for RBC300 and 0.52 for SRBC300, while the Q_m was 1.92 mg N/g for RBC300 and 5.19 mg N/g for SRBC300. After sulfonation, higher O/C mole ratios resulted in greater ammonium adsorption capacities in SRBCs than in the unsulfonated RBCs. It has also been observed that lower temperature produced biochar had both higher O/C mole ratio and ammonium adsorption capacity (Yang et al., 2017), which had the same trends with this study. In addition, the fraction of H decreased from 3.25% for RBC300 to 2.39% for SRBC300, which supports the FTIR analysis and suggests that sulfonation destroys the C–H bond in the aliphatic chain of RBCs, thereby causing the loss of H.

3.4.3. XPS

The XPS spectra of RBC300 and SRBC300 were scanned to observe differences before and after sulfonation (Fig. 5). The low-resolution XPS spectra for RBC300 and SRBC300 (Fig. 5A) showed changes in the biochar's elemental composition upon sulfonation. Accordingly, the sulfuric acid modification introduced more oxygen-bearing functional groups into the SRBC sample, and the oxygen to carbon (O/C) atomic ratio increased from 0.17 to 0.29 post-treatment. The survey scans also suggest that sulfonation resulted in an increase in the atomic percentage of sulfur to approximately 2 at.%. Nitrogen was detected in both biochar samples but at minor levels, that is, 1–2 at.%; nitrogen might have been present in the forms of N–C and N–H groups but not as oxygen-bonded N groups.

The high-resolution XPS data of S 2p, C 1s, and O 1s were deconvoluted to study the bonding states between sulfur, carbon, and oxygen. Quantifications were obtained by applying the Tougaard background correction to these peaks. Our analysis of the high-resolution S 2p scan (Fig. 5B) was indicative of 2 S species in the SRBC300 sample: one S 2p3/2 peak at the binding energy (BE) of 163.8 eV for C–S–C (sulfide) or C–S–H (thiol), and another S2p3/2 peak at the binding energy of 167.9 eV for C–SO_2–C (sulfone) or C–SO_3H (sulfonate). Most of the S was present in the sulfone and/or sulfonate functional group(s) (~92 at.%), while sulfide was only present to a much lesser extent. These peaks agree with those reported in the literature for the S2p3/2 binding energy of organic sulfur compounds. A high-resolution scan of S 2p in RBC300 also showed a small peak around BE 168–170 eV that stemmed from the S content of the precursor material.

Because of the close BEs between the C 1s peaks of graphitic and aromatic carbons (sp3 and sp2 C, respectively), these two carbon bonding states were not deconvoluted into two separate peaks but shared one main peak at 284.8 eV. This is a common charge-correction step for XPS data and for the comparison of XPS data for RBC300 (Fig. 5C) and SRBC300 (Fig. 5D). Accordingly, the C 1s XPS spectrum was deconvoluted into six peaks. For RBC300, C–C/C–H/C═C was the major component (~71 at.%). The presence of aromatic carbon in the sample was also evidenced by the presence of the π–π * satellite peak at several eV beyond the BE of the main peak (~6 eV). Carbon could also have been present in the form of carbonate but only at a small percentage (~2 at.%). Alcohol and ether carbons (C–OH, C–O) were the second most prevalent carbon bonding states for up to 17 at.%. Ketone and carboxylic carbon also existed but at small fractions: ~4 and 3 at.%, respectively. Sulfonation significantly reduced the fraction of C–C/C–H in the SRBC300; aliphatic carbon remained the main component but only occupied ~60 at.%. In contrast, the atomic percentages of carbons bound to oxygen increased accordingly to ~20 at.% for ether, ~7 at.% for ketone, and ~7.7 at.% for carboxylic functional groups. These increases are in agreement with the FTIR findings (Fig. 4), which indicated a higher fraction of the C═O functional group in SRBC300 than in RBC300. The reduction in the main carbon peak of SRBC300 could also be attributed to the sulfonation of aromatic carbon. Furthermore, the reduction in C═C aromatic carbon was coincident with the decline (disappearance) of the π–π* satellite peaks in SRBC300's C 1s spectrum. The O 1s envelope of RBC300 was resolved into four peaks attributed to C-bearing oxygen groups. The O 1s of SRBC300 was deconvoluted into five peaks to account for the presence of C–SO_2–C (sulfone) and/or C–SO_3H (sulfonate), which was consistent with the high-resolution scans of S 2p and C 1s.

3.4.4. Potential mechanisms

From the above characterizations, sulfonation created no additional surface area for biochar. Thus, the enhanced ammonium adsorption can hardly be caused by the increase of surface area. Instead, the FTIR spectra and elemental analyses showed more O-containing functional groups, including –SO_3H and –COOH, on SRBC than on RBC, indicating that sulfonation successfully incorporated such functional groups. Therefore, the chemical interaction or electrostatic attraction between OFGs and ammonium are most likely the main mechanisms to enhance the ammonium adsorption of sulfonated biochar.

Seredych and Bandosz suggested that ammonia may act as a Brønsted or Lewis acid to form amines or amides with OFGs, and the latter acid is more likely to occur in dry environments (Seredych and Bandosz, 2007). According to their study, in the aqueous phase of natural water and

Table 3
Elemental analysis of RBC300 and SRBC300.

Sample	Weight fraction of elements, %						O/C
	C	Mole ratio	O	N	S	Ash	
RBC300	66.21	3.25	18.35	1.18	0.35	10.66	0.21
SRBC300	48.50	2.39	33.44	0.98	2.73	11.96	0.52

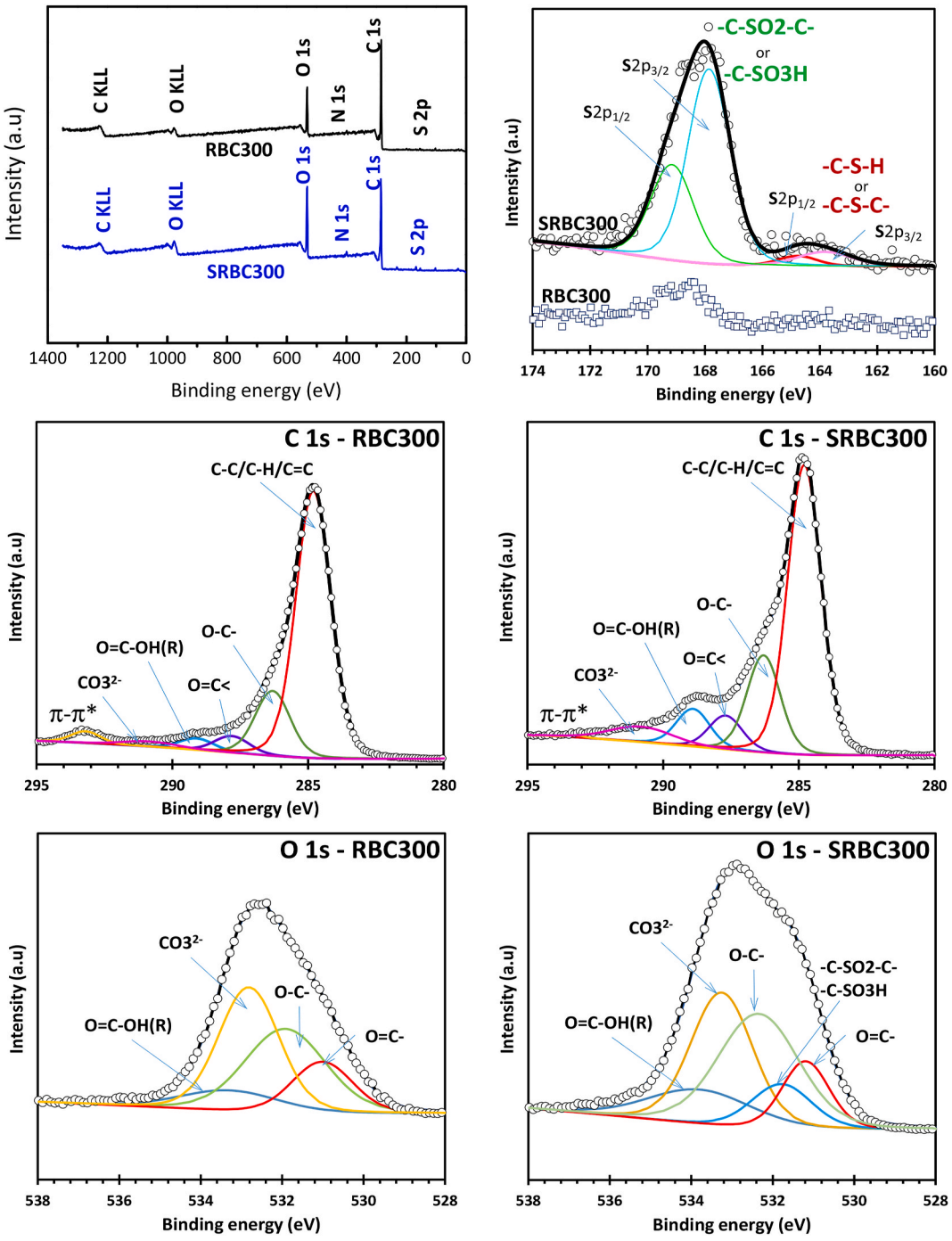

Fig. 5. XPS survey scans of RBC300 and SRBC300, and high-resolution scans of S 2p, C 1s, and O 1s.

wastewater, ammonium is the predominant form of ammonia, and it acts as a Brønsted acid to react with the carboxylic groups:

$$R–COO^- + NH_4^+ = R–COONH_4$$

After sulfonation, new sulfonic groups and more carboxylic groups were formed on the biochar surface, thus significantly enhancing the adsorption of ammonium from water. Detailed mechanisms are demonstrated in the graphical abstract.

$$R–SO_3^- + NH_4^+ = R–SO_3NH_4$$

4. Conclusions

This study performed batch adsorption kinetics and isotherm investigations on both reed biochars (RBCs) and sulfonated reed biochar (SRBCs) to evaluate their potential ammonium removal capacities. The results showed that biochar produced at a lower temperature (300 °C) had much greater ammonium adsorption capacity than those produced at higher temperatures (500 °C and 700 °C), attributed to the higher prevalence of OFGs. The ammonium adsorption rates of SRBCs were much higher, and maximum adsorption capacities were much greater than those of RBCs, indicating that sulfonation can significantly improve the adsorption performance of biochar for ammonium removal. Further characterization of RBC and SRBC revealed that $–SO_3H$ was successfully

introduced on SRBC, and O-containing functional groups, including $–SO_3^-$ and $–COO^-$, increased after sulfonation. Ammonium in water can act as a Brønsted acid and react with carboxylic and sulfonic groups on biochar, which is most likely the main mechanism for the enhancement of ammonium adsorption by sulfonation. Thus, sulfonation could be usefully applied to increase O-containing functional groups and significantly improve biochar ammonium removal. However, the production process, especially the sulfonation, may cause non-ecofriendly issues if it is poorly managed. Besides, all results in this study were obtained in lab-scale batch experiments. Further investigations under field conditions are required to assess the potential application of sulfonated biochars in real water or wastewater environments. The influences of pH, dissolved organic matter, and so on need to be further investigated.

Declaration of competing interest

The authors declare that they have no known competing financial interests or personal relationships that could have appeared to influence the work reported in this paper.

Acknowledgments

The authors thank the financial support by the Fundamental Research Funds for the Central Universities (2020FZZX001-06) and the Cooperative Research Program for Agriculture Science and Technology Development (Project No. PJ01475801), Rural Development Administration, Republic of Korea.

Appendix A. Supplementary data

Supplementary data to this article can be found online at https://doi.org/10.1016/j.envpol.2021.118412.

Credit author statement

Ming Zhang: Conceptualization, Data curation, Formal analysis, Investigation, Methodology, Validation, Visualization, Writing – original draft, Writing – review & editing. Ruyi Sun: Investigation, Visualization, Writing – original draft. Ge Song: Conceptualization, Resources, Writing – review & editing. Lijun Wu: Formal analysis, Validation, Writing – review & editing. Hui Ye: Formal analysis, Validation, Writing – review & editing. Liheng Xu: Formal analysis, Validation, Writing – review & editing. Sanjai J.Parikh: Conceptualization, Writing – review & editing. Tuan Nguyen: Formal analysis, Methodology. Eakalak Khan: Conceptualization, Writing – review & editing. Meththika vithanage: Conceptualization, Writing – review & editing. Yong Sik Ok: Conceptualization, Funding acquisition, Methodology, Project administration, Resources, Supervision, Writing – original draft, Writing – review & editing.

References

Ahmad, M., Rajapaksha, A.U., Lim, J.E., Zhang, M., Bolan, N., Mohan, D., Vithanage, M., Lee, S.S., Ok, Y.S., 2014. 'Biochar as a sorbent for contaminant management in soil and water: a review. Chemosphere 99, 19–33.

Alshameri, A., He, H.P., Zhu, J.X., Xi, Y.F., Zhu, R.L., Ma, L.Y., Tao, Q., 2018. 'Adsorption of ammonium by different natural clay minerals: characterization, kinetics and adsorption isotherms. Appl. Clay Sci. 159, 83–93.

Brancaleon, L., Bamberg, M.P., Sakamaki, T., Kollias, N., 2001. 'Attenuated total reflection-fourier transform infrared spectroscopy as a possible method to investigate biophysical parameters of stratum corneum in vivo. J. Invest. Dermatol. 116, 380–386.

Cao, L.C., Yu, I.K.M., Chen, S.S., Tsang, D.C.W., Wang, L., Xiong, X.N., Zhang, S.C., Ok, Y. S., Kwon, E.E., Song, H., Poon, C.S., 2018. 'Production of 5-hydroxymethylfurfural from starch-rich food waste catalyzed by sulfonated biochar. Bioresour. Technol. 252, 76–82.

Chen, L., Chen, X.L., Zhou, C.H., Yang, H.M., Ji, S.F., Tong, D.S., Zhong, Z.K., Yu, W.H., Chu, M.Q., 2017. 'Environmental-friendly montmorillonite-biochar composites: facile production and tunable adsorption-release of ammonium and phosphate. J. Clean. Prod. 156, 648–659.

Conley, D.J., Paerl, H.W., Howarth, R.W., Boesch, D.F., Seitzinger, S.P., Havens, K.E., Lancelot, C., Likens, G.E., 2009. Controlling eutrophication: nitrogen and phosphorus. Science 323, 1014–1015.

Fan, R.M., Chen, C.L., Lin, J.Y., Tzeng, J.H., Huang, C.P., Dong, C.D., Huang, C.P., 2019. 'Adsorption characteristics of ammonium ion onto hydrous biochars in dilute aqueous solutions. Bioresour. Technol. 272, 465–472.

Gai, X.P., Wang, H.Y., Liu, J., Zhai, L.M., Liu, S., Ren, T.Z., Liu, H.B., 2014. 'Effects of feedstock and pyrolysis temperature on biochar adsorption of ammonium and nitrate. PLoS One 9, e113888.

Gong, Y.P., Ni, Z.Y., Xiong, Z.Z., Cheng, L.H., Xu, X.H., 2017. 'Phosphate and ammonium adsorption of the modified biochar based on Phragmites australis after phytoremediation. Environ. Sci. Pollut. Res. 24, 8326–8335.

Hafner, S.C., Parikh, S.J., 2020. 'Sorption and abiotic transformation of monensin by iron and manganese oxides. Chemosphere 253.

Hale, S.E., Alling, V., Martinsen, V., Mulder, J., Breedveld, G.D., Cornelissen, G., 2013. 'The sorption and desorption of phosphate-P, ammonium-N and nitrate-N in cacao shell and corn cob biochars. Chemosphere 91, 1612–1619.

Hidayat, A., Rochmadi, K. Wijaya, Budiman, A., 2015. Reaction kinetics of free fatty acids esterification in palm fatty acid distillate using coconut shell biochar sulfonated catalyst. Int. Conf. Chem. Mater. Eng. (Iccme) 2015: Green Technol. Sustain. Chem. Prod. Proc. 1699, 050005.

Ho, Y.S., 1995. Adsorption of Heavy Metals from Waste Streams by Peat. University of Birmingham.

Ho, Y.S., McKay, G., 1999. 'Pseudo-second order model for sorption processes. Process Biochem. 34, 451–465.

Hou, J., Huang, L., Yang, Z., Zhao, Y., Deng, C., Chen, Y., Li, X., 2016. Adsorption of ammonium on biochar prepared from giant reed. Environ. Sci. Pollut. Res. Int. 23, 19107–19115.

Hsu, J.H., Lo, S.L., 1999. 'Chemical and spectroscopic analysis of organic matter transformations during composting of pig manure. Environ. Pollut. 104, 189–196.

Ismadji, S., Tong, D.S., Soetaredjo, F.E., Ayucitra, A., Yu, W.H., Zhou, C.H., 2015. 'Bentonite hydrochar composite for removal of ammonium from Koi fish tank. Appl. Clay Sci. 119, 146–154.

Jorgensen, T.C., Weatherley, L.R., 2003. Ammonia removal from wastewater by ion exchange in the presence of organic contaminants. Water Res. 37, 1723–1728.

Kang, S., Xing, B., 2007. 'Adsorption of dicarboxylic acids by clay minerals as examined by in situ ATR-FTIR and ex situ DRIFT. Langmuir 23, 7024–7031.

Keiluweit, M., Nico, P.S., Johnson, M.G., Kleber, M., 2010. Dynamic molecular structure of plant biomass-derived black carbon (biochar). Environ. Sci. Technol. 44, 1247–1253.

Kizito, S., Wu, S., Kipkemoi Kirui, W., Lei, M., Lu, Q., Bah, H., Dong, R., 2015. 'Evaluation of slow pyrolyzed wood and rice husks biochar for adsorption of ammonium nitrogen from piggery manure anaerobic digestate slurry. Sci. Total Environ. 505, 102–112.

Lagergren, S., 1898. 'About the theory of so-called adsorption of soluble substances. K. - Sven. Vetenskapsakademiens Handl. 24, 1–39.

Maranon, E., Ulmanu, M., Fernandez, Y., Anger, I., Castrillon, L., 2006. Removal of ammonium from aqueous solutions with volcanic tuff. J. Hazard Mater. 137, 1402–1409.

Ministry of Environmental Protection, 2009. Water Quality. Determination of Ammonia Nitrogen. Salicylic Acid Spectrophotometry. China Environmental Science Press, Beijing.

Niu, Y.C., Zhao, Y., Xi, B.D., Hu, X., Xia, X.F., Wang, L., Lv, D.D., Lu, J.J., 2012. 'Removal of ammonium from aqueous solutions using synthetic zeolite obtained from coal fly-ash. Fresenius Environ. Bull. 21, 1732–1739.

Ozcimen, D., Ersoy-Mericboyu, A., 2010. 'Characterization of biochar and bio-oil samples obtained from carbonization of various biomass materials. Renew. Energy 35, 1319–1324.

Parikh, S.J., Goyne, K.W., Margenot, A.J., Mukome, F.N.D., Calderon, F.J., 2014. 'Soil chemical insights provided through vibrational spectroscopy. Adv. Agron. 126, 1–148.

Peak, D., Ford, R.G., Sparks, D.L., 1999. 'An in situ ATR-FTIR investigation of sulfate bonding mechanisms on goethite. J. Colloid Interface Sci. 218, 289–299.

Seredych, M., Bandosz, T.J., 2007. 'Mechanism of ammonia retention on graphite oxides: role of surface chemistry and structure. J. Phys. Chem. C 111, 15596–15604.

Sharma, R.K., Wooten, J.B., Baliga, V., Lin, X.H., Chan, W.G., Hajaligol, M.R., 2004. Characterization of chars from pyrolysis of lignin. Fuel 83, 1469–1482.

Woodward, G., Gessner, M.O., Giller, P.S., Gulis, V., Hladyz, S., Lecerf, A., Malmqvist, B., McKie, B.G., Tiegs, S.D., Cariss, H., Dobson, M., Elosegi, A., Ferreira, V., Graca, M.A. S., Fleituch, T., Lacoursiere, J.O., Nistorescu, M., Pozo, J., Risnoveanu, G., Schindler, M., Vadineanu, A., Vought, L.B.M., Chauvet, E., 2012. Continental-scale effects of nutrient pollution on stream ecosystem functioning. Science 336, 1438–1440.

Xia, Y.F., Zhang, M., Tsang, D.C.W., Geng, N., Lu, D.B., Zhu, L.F., Igalavithana, A.D., Dissanayake, P.D., Rinklebe, J., Yang, X., Ok, Y.S., 2020. 'Recent advances in control technologies for non-point source pollution with nitrogen and phosphorous from agricultural runoff: current practices and future prospects. Appl. Biol. Chem. 63, 8.

Xiong, X.N., Yu, I.K.M., Chen, S.S., Tsang, D.C.W., Cao, L.C., Song, H., Kwon, E.E., Ok, Y. S., Zhang, S.C., Poon, C.S., 2018. 'Sulfonated biochar as acid catalyst for sugar hydrolysis and dehydration. Catal. Today 314, 52–61.

Yang, H.I., Lou, K., Rajapaksha, A.U., Ok, Y.S., Anyia, A.O., Chang, S.X., 2017. 'Adsorption of ammonium in aqueous solutions by pine sawdust and wheat straw biochars. Environ. Sci. Pollut. Res. 8, 25638–25647.

Yang, W., Li, A., Fu, C., Fan, J., Zhang, Q., 2007. 'Adsorption mechanism of aromatic sulfonates onto resins with different matrices. Ind. Eng. Chem. Res. 46, 6971–6977.

Zeng, Z., Zhang, S.D., Li, T.Q., Zhao, F.L., He, Z.L., Zhao, H.P., Yang, X.E., Wang, H.L., Zhao, J., Rafiq, M.T., 2013. 'Sorption of ammonium and phosphate from aqueous solution by biochar derived from phytoremediation plants. J. Zhejiang Univ. - Sci. B 14, 1152–1161.

Zhang, Ming, Song, Ge, Gelardi, Danielle L., Huang, Longbin, Khan, Eakalak, Masek, Ondrej, Parikh, Sanjai J., Yong Sik, Ok, 2020. 'Evaluating biochar and its modifications for the removal of ammonium, nitrate, and phosphate in water. Water Res. 186, 116303-03.

Zhang, T., Li, Q.C., Ding, L.L., Ren, H.Q., Xu, K., Wu, Y.G., Sheng, D., 2011. 'Modeling assessment for ammonium nitrogen recovery from wastewater by chemical precipitation. J. Environ. Sci. 23, 881–890.

Zheng, H., Wang, Z.Y., Deng, X., Zhao, J., Luo, Y., Novak, J., Herbert, S., Xing, B.S., 2013. 'Characteristics and nutrient values of biochars produced from giant reed at different temperatures. Bioresour. Technol. 130, 463–471.